

# Numerical Investigation of the Chilling of Food Products by Air-Mist Spray

Roy J. Issa

**Abstract**—Spray chilling using air-mist nozzles has received much attention in the food processing industry because of the benefits it has shown over forced air convection. These benefits include an increase in the heat transfer coefficient and a reduction in the water loss by the product during cooling. However, few studies have simulated the heat transfer and aerodynamics phenomena of the air-mist chilling process for optimal operating conditions. The study provides insight into the optimal conditions for spray impaction, heat transfer efficiency and control of surface flooding. A computational fluid dynamics model using a two-phase flow composed of water droplets injected with air is developed to simulate the air-mist chilling of food products. The model takes into consideration droplet-to-surface interaction, water-film accumulation and surface runoff. The results of this study lead to a better understanding of the heat transfer enhancement, water conservation, and to a clear direction for the optimal design of air-mist chilling systems that can be used in commercial applications in the food and meat processing industries.

**Keywords**—Droplets impaction efficiency, Droplet size, Heat transfer enhancement factor, Water runoff.

## I. INTRODUCTION

COOLING by air-mist sprays has been commercially used in many applications in the food processing industry because of the heat transfer benefits it has shown over conventional forced air cooling, but very few studies have been conducted to optimize the amount of water used while maintaining a high cooling efficiency. Alvarez and Flick [1, 2], Ansari and Khan [3], Chuntranuluck et al. [4], and Dirita et al. [5] used forced air flow alone in the cooling of agricultural products and have analyzed the flow dynamics and the heat transfer of the cooling process. Other researchers such as Allais et al. [6], and Allais and Alvarez [7] conducted heat transfer studies using sprays dispersing air and water droplets in the cooling of food products (Fig. 1-a). Their studies showed that cooling using a multi-phase flow can enhance the cooling process by a maximum factor of about 2.8. Their air-mist sprays dispersed very fine droplets that are less than 10  $\mu\text{m}$  in size. Abdul-Majeed [8] conducted studies on hydrair cooling that uses water droplets greater than 100  $\mu\text{m}$  in the cooling of food products. It was reported that hydrair cooling is most effective at lower water-film Reynolds numbers.

R. J. Issa is an assistant professor of Mechanical Engineering, West Texas A&M University, Canyon, TX 79016 USA (phone: 806-651-5261; fax: 806-651-5259; e-mail: rissa@mail.wtamu.edu).

In the research for beef carcass air-assisted spray chilling (Fig. 1-b), computer modeling [9, 10] and experimental [11-13] studies have been conducted to investigate the effect of using a two phase flow on the chilling process. A variety of chilling techniques have been adopted by researchers that range from using conventional air chilling systems [9] to air-assisted chilling systems with a variety of intermittent cooling schemes [12, 13]. In these studies, the amount of water used to cool the beef carcass ranged from 3.5 to 7 gallons per carcass and for spray cooling periods from 10 to 17 hours. However, none of those researchers have examined the effect of using nozzles producing different droplet sizes. Most of them have used nozzles producing large size droplets such as full jets nozzles (1140-4300  $\mu\text{m}$  average drop size) and hollow cone nozzles (360-3400  $\mu\text{m}$  average drop size). These large size droplets result in poor cooling efficiency and in an increase in the water run-off and over-spray onto the target surface.

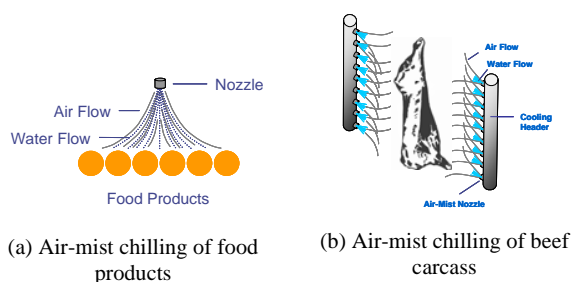


Fig. 1 Air-mist chilling applications

There is supporting evidence that shows the droplet size in the spray has a strong effect on the heat transfer enhancement [14]. Results have shown that decreasing the droplets size from 100 to 50  $\mu\text{m}$  can result in water savings between 20-30%. The heat transfer from the spray is very much dependent on two major parameters: the impinging droplet size and the water mass flow flux (mass flow rate per contact surface area). The smaller the droplet size, the easier it is for the droplet to evaporate on the surface; thus leading to higher heat transfer enhancement. Also, smaller size droplets will better cool the thermal boundary layer near the surface by increasing the near surface local vapor convection. However, a higher water mass flow flux or large size droplets will have a detrimental effect on the surface cooling because of the

surface flooding that can occur. If the spray droplets are too large, there is a risk of water running down the target surface. This will have a detrimental effect on the quality of the processed product due to the bleached marks that can be produced on the surface.

The objective of this research is to numerically simulate using computational fluid dynamics the air-mist chilling of food products. This consists of conducting parametric studies to provide an insight into: 1) the optimal droplet size required to achieve maximum cooling, 2) the optimal droplet size required to maximize the spray impaction efficiency, and 3) and the spray duration and frequency that need to be adopted in the chilling process to minimize the amount of water over-spray on the target surface. Besides the spray droplet size, simulations are needed to show the dependence of the air-mist spray heat transfer and droplets dynamics on other factors such as: air-to-liquid loading, air and water flow rates, relative humidity, surface temperature, and nozzle-to-surface distance. The benefits of this research are: a reduction in the amount of water used in spray chilling applications in the food processing industry, a reduction in surface flooding and in the amount of waste water causing contamination.

## II. SPRAY IMPACTION

The spray impaction efficiency,  $\eta$ , is defined as the ratio of the actual mass flow flux of the droplets deposited onto the target surface to the maximum droplets mass flow flux leaving the nozzle exit. This is expressed as:

$$\eta = \frac{G}{G_{\max}} \quad (1)$$

There are several factors that influence the spray impaction on the target surface (Fig. 2). These include: droplet diameter, spray orientation, water flow rate, air-to-liquid loading, nozzle-to-surface distance, relative humidity, and surface temperature.

Spray impaction is strongly influenced by the droplets size in the spray [15, 16]. Sprays with large droplets have high impaction efficiency. As the large droplets exit the nozzle, they will continue to follow their own trajectories and will not be caught up in the air stream as they get near the surface. On the other hand, small size droplets will have difficulty staying the course of their initial trajectory and will simply drift away along the air stream as they approach the surface.

Other factors that influence the droplets movement and eventually affect the droplets impaction on the target surface include air-to-liquid loading ratio and water mass flow rate. The air-to-liquid loading is defined as the ratio of air mass flow rate to water mass flow rate. The size of the droplets produced by an air-assisted nozzle is controlled by the nozzle's air and water operating pressures. Small size droplets can be generated by either increasing the air pressure while decreasing the liquid pressure, or by increasing the air flow rate while decreasing the liquid flow rate. An increase in

TABLE I  
NOMENCLATURE

Symbol	Definition	Units
$A$	Chilled surface area	$m^2$
$A_d$	Droplet surface area	$m^2$
$c_{p,l}$	Liquid droplet specific heat constant	J/kg.K
$D$	Target surface diameter	m
$d$	Droplet diameter	m ( $\mu$ m)
$\vec{F}$	External force per unit mass acting on droplet	$m/s^2$
$F_D$	Drag force coefficient	1/s
$f_i$	Weighing factor for heat transfer enhancement	
$f_s$	Weighing factor for droplets impaction efficiency	
$\vec{g}$	Gravitational acceleration vector	$m/s^2$
$G$	Water mass flow flux (actual)	$kg/m^2.s$
$G_{\max}$	Maximum water mass flow flux	$kg/m^2.s$
$H$	Nozzle-to-surface distance	m
$h_a$	Bulk air heat transfer coefficient	W/m <sup>2</sup> .K
$h_{fg}$	Latent heat of vaporization	J/kg
$m_d$	Droplet mass	kg
$\dot{m}_w$	Mass flow rate of impinging droplets	kg/s (gph)
$\dot{m}_e$	Droplet evaporation mass flow rate	kg/s
$P$	Multiple-objective parameter	
$\dot{q}_a$	Air heat transfer	W
$\dot{q}_{total}$	Total heat transfer	W
$Sto$	Stokes number	
$S_\Phi$	General source term	
$S_{\Phi d}$	Source term due to the droplets presence	
$t$	Time	s
$T_s$	Chilled surface temperature	$^{\circ}$ C
$T_\infty$	Ambient (air) temperature	$^{\circ}$ C
$T_d$	Droplet temperature	$^{\circ}$ C
$\vec{U}$	Transport velocity vector	m/s
$\vec{v}_a$	Air velocity vector	m/s
$\vec{v}_d$	Droplet velocity vector	m/s
$\varepsilon$	Spray heat transfer enhancement factor	
$\Gamma$	Transport diffusivity	$m^2/s$
$\phi$	Relative humidity	
$\psi$	Air-to-water mass flow rate loading ratio	
$\Phi$	Dependant variable	
$\nabla$	Gradient operator	
$\eta$	Droplets impaction efficiency	
$\rho_a$	Air density	$kg/m^3$
$\rho_d$	Droplet density	$kg/m^3$
$\mu_a$	Air dynamic viscosity	$kg/s.m$

the pressure difference between the liquid and air will result in an increase in the relative velocity between them. This leads to an increase in the shear force acting on the liquid film, and as a result, finer droplets can be generated. Increasing the air mass flow rate while keeping the water mass flow rate the same will result in an increase in the droplets momentum which leads to an increase in the droplets impaction efficiency. On the other hand, increasing the water mass flow rate (for the same amount of air mass flow rate) will result in an increase in the number of droplets, droplet-to-droplet interaction, and in the amount of surface flooding.

An increase in the nozzle-to-surface distance will lead to a decrease in the droplet impaction velocity due to the longer duration the drag force will be acting on the droplet. With

less momentum, the droplets surface impaction efficiency will decrease. Surface and ambient temperature and relative humidity also affect the droplet impaction. An increase in the target surface or ambient temperature will result in an increase in the droplet evaporation. This leads to more droplets drifting away due to the continuously shrinking droplet diameter, and therefore, lowers the impaction efficiency. Finally, the increase in relative humidity tends to have a favorable effect on the spray impaction efficiency. This is due to the lower evaporation rates which result in droplets reaching the target surface with higher impinging velocities.

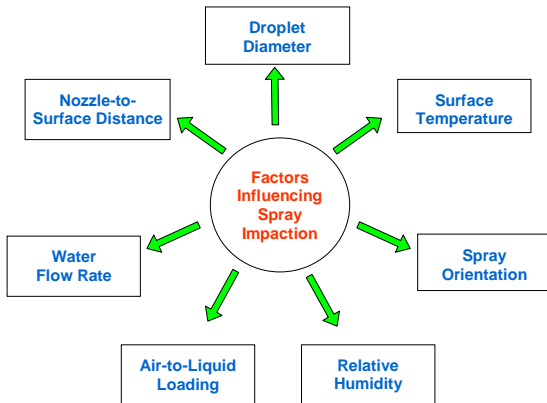


Fig. 2 Factors influencing air-mist chilling

### III. SPRAY HEAT TRANSFER

There are three modes of heat transfer associated with the air-mist spray chilling of surfaces slightly heated to temperatures above room temperature. These are: 1) convection heat transfer associated with the bulk air flow, 2) evaporation heat transfer of the droplets while being airborne and also on the target surface, and 3) sensible heat transfer associated with the droplets contact with the heated surface. The total heat flux can be expressed as:

$$\dot{q}_{total} = h_a A(T_s - T_\infty) + \dot{m}_e h_{fg} + \dot{m}_w c_{p,l}(T_s - T_\infty) \quad (2)$$

The spray heat transfer enhancement factor,  $\varepsilon$ , is defined as the ratio of the heat transfer of the two-phase flow (air and water) to the heat transfer of the single-phase flow (air alone):

$$\varepsilon = \frac{\dot{q}_{total}}{\dot{q}_a} \quad (3)$$

Sprays using air and water are more efficient than those using water alone. This is because air injected with water increases the droplets momentum and enhances the impaction. The more the droplet spreads during impaction, the higher is the heat transfer enhancement due to the increase in the contact interface between the liquid droplet and the solid surface [17, 18]. For sufficiently high incoming droplet

momentum, better droplet-to-surface contact and therefore better surface wetting can be established as long as surface flooding is minimized. Surface flooding is detrimental to the cooling effectiveness due to the increase in droplet-to-droplet interaction.

If fine size droplets make it to the surface, the droplets momentum on impaction will be so weak (compared to the surface tension force) that the droplets can easily adhere to the surface. However, very fine droplets are not recommended because they can easily drift away and may never reach the target surface. On the other hand, droplets should not be too large because the larger the droplets the more difficult it is for them to evaporate and effectively cool the surface. Also, large size droplets provide non-uniform cooling. Therefore, optimal size droplets need to be determined.

### IV. NUMERICAL MODEL

A 2-D numerical model for the air-mist chilling of food products is developed using FLUENT, a commercially available computational fluid dynamics toolbox. To model the transport phenomenon of the multi-phase flow, the droplets are modeled in the Lagrangian frame of reference, and are dispersed stochastically in the continuous gas phase. The turbulence continuous phase model uses the two equations in the k- $\varepsilon$  method expressed in Eulerian coordinates. The effect of the gas turbulence on the droplets is obtained by adding a velocity fluctuation to the mean gas velocity while tracing the droplets. The fluctuating velocity components, which are discrete piecewise functions of time, have their random value constant over an interval of time given by the characteristic lifetime of the eddies. The general form of the continuous phase equation for the energy, momentum, turbulence kinetic energy, and energy dissipation rate of the turbulent kinetic energy is:

$$\frac{\partial}{\partial t}(\rho_a \Phi) + \nabla \cdot (\rho_a \vec{U} \Phi) = \nabla \cdot (\Gamma \nabla \Phi) + S_\Phi + S_{\Phi d} \quad (4)$$

Where  $\Phi = 1, v_x, v_y, v_z, h, k$  and  $\varepsilon$  stands for the continuity, x-momentum, y-momentum, z-momentum, energy, turbulent kinetic energy, and turbulent dissipation rate. Coupling between the liquid droplet phase and the gas phase medium is accomplished by the source terms shown in Eqn. (4). A first-order upwind scheme is applied to the momentum, turbulent kinetic energy, and turbulent kinetic energy dissipation, while the SIMPLE (Semi-Implicit Method for Pressure-Linked Equations) algorithm is employed to enhance the velocity-pressure coupling.

The droplet trajectory is solved by integrating the force balance on the droplet, where the inertial force is balanced by the drag and gravitational forces:

$$\frac{d\vec{v}_d}{dt} = F_D(\vec{v}_a - \vec{v}_d) + \frac{\vec{g}(\rho_d - \rho_a)}{\rho_d} + \vec{F} \quad (5)$$

The droplet temperature is calculated from an energy balance on the droplet, where the sensible heat change in the droplet is balanced by the convective and latent heat transfer between the droplet (discrete phase) and the gas phase (continuous phase) medium:

$$m_d c_{p,l} \frac{dT_d}{dt} = h_a A_d (T_\infty - T_d) + \frac{dm_d}{dt} h_{fg} \quad (6)$$

In the simulation, the nozzle disperses air and water droplets from a round orifice. It is assumed that the water has been fully atomized by the time it exists the nozzle. This simplification is necessary to avoid the need for a complicated model of the nozzle. A 180x60 quadrilateral mesh is generated for the computation domain as shown in Fig. 3. Weighting factors are used to concentrate the grid mesh at the center of the computation domain, and near the plate surface. Sufficient grid refinement at the wall is necessary to capture the wall interaction event and to ensure computational stability.

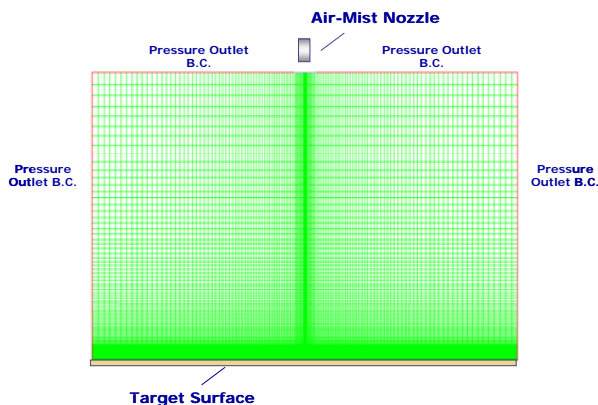


Fig. 3 Grid Mesh of Computation Domain

The boundary conditions for the computation domain are as follows. Velocity inlet boundary conditions are applied at the water droplets and air injection plane. The injection plane is considered to be at a small distance below the nozzle exit plane where the droplets are released. At the vertical edges and top side of the computation domain, pressure outlet boundary conditions are applied. A wall boundary condition is applied at the chilled surface. The model takes into consideration droplet-to-surface interaction and water-film accumulation. According to Stanton and Rutland [19] the impinging droplet can either stick, rebound, or splash at the surface depending on the impinging droplet Weber number. Sticking occurs when the impinging droplet Weber number is less than 16, while splashing occurs when the droplet Weber number is close to or above 60. Between these critical Weber numbers the droplet will bounce on the surface. Stream-lines for the continuous gas phase are shown in Fig. 4 for a typical air-mist spray simulation. The multiphase flow exiting the nozzle causes more air to be withdrawn towards the center of

the spray from the top, right and left sides of the computational domain as shown in the figure below. Circulation regions are shown downstream of the flow towards the target surface and away from the stagnation point.

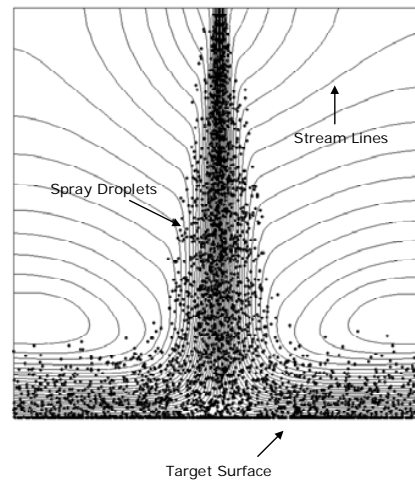


Fig. 4 Typical simulation for spray flow over a target surface

## V. RESULTS AND DISCUSSIONS

### A. Spray Impaction Efficiency

Simulation results presented in this study attempt to give a general description of the transportation process of the impacting sprays onto a target surface as function of the spray median droplet diameter, water flow rate, air-to-liquid loading, nozzle-to-surface distance and relative humidity. Simulations runs are conducted using a full cone nozzle that disperses water droplets injected with air onto a circular surface having a diameter of 0.3 m. Table II shows the test cases conducted in this study and Fig. 5 shows the dimensions associated with the spray configuration.

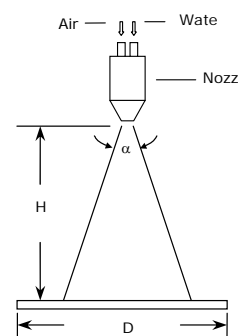


Fig. 5 Spray configuration

TABLE II  
OPERATING CONDITIONS FOR THE TEST CASE RUNS

Case no.	$v_a$ (m/s)	$\dot{m}_w$ (gph)	$\psi$	$H$ (m)	$H/D$
1	6	0.36	1	0.15	0.5
2	6	0.036	10	0.15	0.5
3	63	3.6	1	0.15	0.5
4	63	0.36	10	0.15	0.5
5	6	0.36	1	0.30	1
6	6	0.036	10	0.30	1
7	63	3.6	1	0.30	1
8	63	0.36	10	0.30	1
9	6	0.36	1	0.60	2
10	6	0.036	10	0.60	2
11	63	3.6	1	0.60	2
12	63	0.36	10	0.60	2

Figs. 6(a), 6(b) and 6(c) show the droplet impaction efficiency for nozzle-to-surface distances of 0.15, 0.3 and 0.6 m, respectively. The relative humidity for these cases is 1. Two cases of 1 and 10 air-to-liquid loadings are shown. For the case of air-to-liquid loading of 1, water flow rates of 0.36 and 3.6 gph are simulated, and for the case of air-to-liquid loading of 10, water flow rates of 0.036 and 0.36 gph are simulated. For the same amount of air and water mass flow rates, sprays with larger droplets have lower droplet number density but higher droplet momentum. More droplets make impaction at the plate than when finer droplets are dispersed, and the number of drifting droplets decreases sharply. For the same amount of water flow rate and same water droplets size, as the air-to-liquid loading increases (such as by introducing an auxiliary air flow to enhance in pushing the droplets further away downstream) the impaction efficiency drastically increases due to the increase in the droplets impinging velocity and momentum. On the other hand, for the same amount of air flow rate and same water droplets size, as the water flow rate increases, the impaction efficiency is seen to increase slightly due to the increase in the number of water droplets causing fewer droplets to drift away before hitting the target surface. However, the effect from the increase in air flow rate is stronger than that of the increase in water flow rate for the same droplets size.

Comparing Figs. 6(a) through 6(c) for the different nozzle-to-surface distances, the droplet impaction efficiency sharply decreases as the nozzle-to-surface distance increases for sprays having droplets less than 30  $\mu\text{m}$ . Impaction efficiencies higher than 95% were achieved when sprays disperse droplets greater than or equal to 50  $\mu\text{m}$  for nozzle-to-surface distances between 0.15 and 0.3 m. However, for a nozzle-to-surface distance around 0.6 m, impaction efficiencies higher than 90% were achieved when sprays disperse droplets that are 70  $\mu\text{m}$  or larger in diameter. As the nozzle-to-surface distance increases, larger droplets are needed to achieve high impaction efficiency.

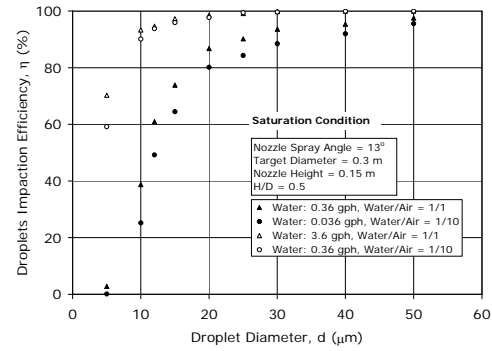


Fig. 6 (a) Droplets impaction efficiency versus droplet diameter  
( $\phi = 1$ ,  $H = 0.15$  m,  $D = 0.3$  m)

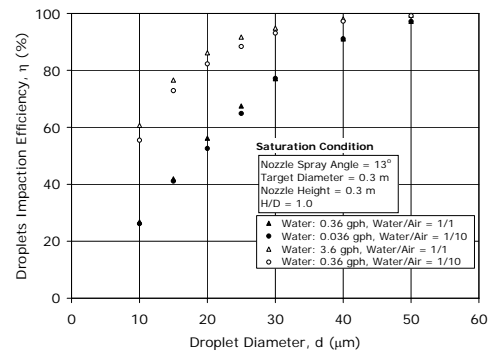


Fig. 6 (b) Droplets impaction efficiency versus droplet diameter  
( $\phi = 1$ ,  $H = 0.3$  m,  $D = 0.3$  m)

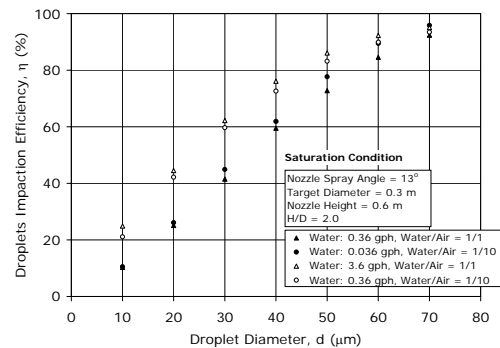


Fig. 6 (c) Droplets impaction efficiency versus droplet diameter  
( $\phi = 1$ ,  $H = 0.6$  m,  $D = 0.3$  m)

The effect of humidity on the spray impaction efficiency is clearly visible in Figs. 7(a) through 7(c). Two extreme cases are shown: saturated ( $\phi=1$ ) and dry ( $\phi=0$ ) ambient conditions. For the case of dry ambient condition, droplets evaporation occurs very rapidly such that droplets may completely evaporate before reaching the surface. As a result, the droplets impaction efficiency significantly decreases. This is strongly evident in the case of large nozzle-to-surface distances as seen in Fig. 7(c). As the nozzle-to-surface distance decreases, droplets evaporation reduces which leads

to an increase in impaction efficiency. For the same amount of air flow rate and initial droplet size, as the water flow rate increases the impaction efficiency improves significantly for the dry case. This is because the increase in water flow rate increases the vapor concentration. The rate of evaporation is governed by the gradient of the vapor concentration between the droplet and the bulk air. For the case of a saturated ambient, the impaction efficiency slightly increases when the water flow rate increases for nozzle-to-surface distances of 0.15 and 0.3 m. However when the nozzle-to-surface distance is 0.6 m, the increase in water flow rate results in a slight decrease in the droplet impaction efficiency. This could be due to the increase in droplets concentration pushing the droplets away from the spray center, and since the nozzle is at a larger distance from the target surface, many of the droplets escape the computation domain before reaching the surface.

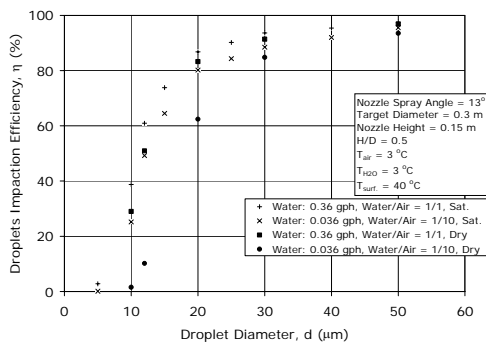


Fig. 7 (a) Droplets impaction efficiency – a comparison between dry and saturated case ( $H = 0.15$  m,  $D = 0.3$  m)

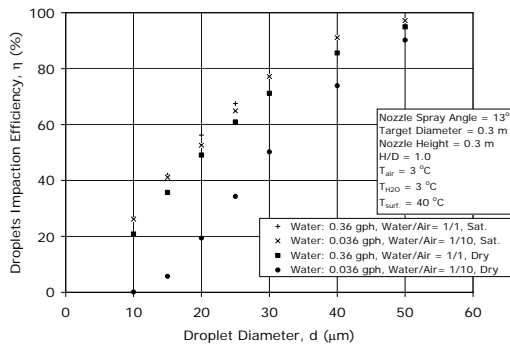


Fig. 7 (b) Droplets impaction efficiency – a comparison between dry and saturated case ( $H = 0.3$  m,  $D = 0.3$  m)

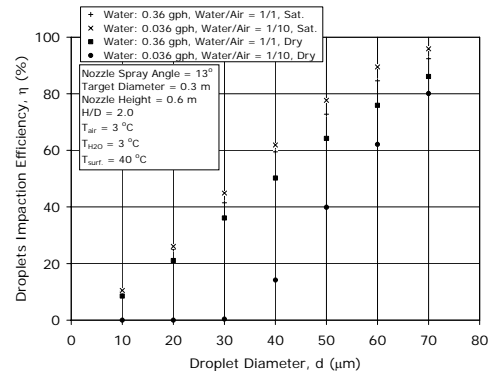


Fig. 7 (c) Droplets impaction efficiency – a comparison between dry and saturated case ( $H = 0.6$  m,  $D = 0.3$  m)

In summary, the impaction efficiency of the droplets is seen to be dependent not only on the droplet diameter, but also on other factors such as: air velocity ( $v_a$ ), water mass flow rate ( $\dot{m}_w$ ), air-to-liquid loading ( $\psi$ ), relative humidity ( $\phi$ ), nozzle-to-surface distance ( $H$ ), and target surface diameter ( $D$ ):

$$\eta = f(d, v_a, \dot{m}_w, \psi, \phi, H, D) \quad (7)$$

The droplets impaction efficiency can also be expressed as function of the Stokes number to assess the probability of droplets making impaction on to the target surface. Stokes number is a non-dimensional parameter that is proportional to the ratio of the droplet stopping distance (distance the droplet moves before it is stationary relative to the fluid) to the target surface diameter:

$$Sto = \frac{2v_a d^2 \rho_d}{18\mu_a D} \quad (8)$$

The simulation results for several test cases are compiled together in Figs. 8(a) and 8(b) for the relative humidity of 1 and 0, and nozzle distance to surface diameter ratio,  $H/D$ , of 0.5, and 2. When saturation conditions prevail, and  $H/D$  is 0.5, the effect of Stokes number on the impaction efficiency is less dependent on other factors such as air and water loadings. However, for cases with higher  $H/D$  ratios, the effect of Stokes number on the impaction efficiency is seen to be strongly dependent on the air mass flow rate (or air velocity). This is apparent in the wide separation in the data associated with case runs where  $H/D$  is greater than 1. For the same Stokes number and lower incoming air velocities, higher droplet diameters result in better impaction efficiency. Also, for the same Stokes number, higher water-to-air loadings in general result in better impaction efficiency. As the relative humidity decreases, the effect of Stokes number on the impaction efficiency becomes even more strongly dependent on the air and water loadings as shown in Fig. 8(b).

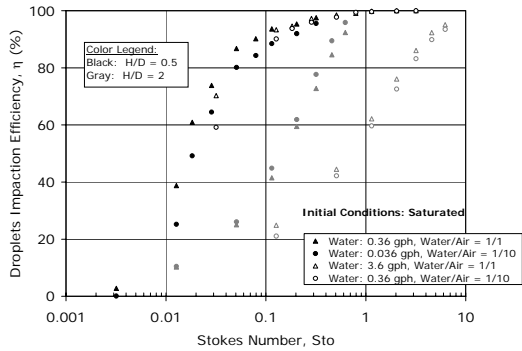


Fig. 8 (a) Droplets impaction efficiency versus Stokes number (Comparison between saturated case runs,  $\phi=1$ )

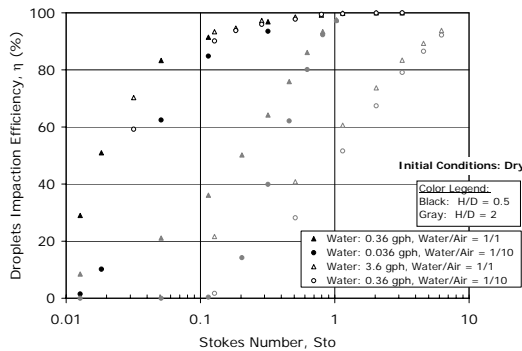


Fig. 8 (b) Droplets impaction efficiency versus Stokes number (Comparison between dry case runs,  $\phi=0$ )

### B. Heat Transfer Enhancement

One of the challenges in air mist cooling is to understand the effect of the droplet size on the heat transfer enhancement. As shown earlier, the droplet size is an important factor because it affects the amount of water deposition on the surface. Other factors such as the nozzle-to-surface distance, humidity level, water mass flow rate, and air-to-liquid loading will also affect the heat transfer. Since in air-mist chilling the cooling medium is a two-phase flow (air and discrete water droplets), the first question to be addressed is what desirable droplet size is required for best heat transfer enhancement. Also, in order to reduce the amount of water loss from dehydration by the product during cooling (as in the case of beef carcass cooling), it is important to maximize droplets impaction to create a thin water film on the target surface. The second question to be addressed is what desirable droplet size is best suited to achieve both maximum heat transfer and surface wetting capability.

The effect of the droplet size on both the heat transfer enhancement and impaction efficiency is simulated for nozzle-to-spray distances of 0.15, 0.3, and 0.6 m as shown in Figs. 9(a) through 9(f). Results are presented for two water flow rates and air-to-liquid loadings. The figures show the heat transfer enhancement reaches a maximum for certain droplets size depending on the flow conditions and nozzle-to-surface

distance. The droplets can not be too large because larger droplets have low cooling effectiveness. On the other hand, the droplets can not be too small because they can easily drift away and evaporate before reaching the surface. The required droplets should be of optimal size to evaporate at the surface. For the case where the water flow rate is 0.36 gph and air-to-liquid loading ratio is 1, the optimal droplet size to achieve maximum cooling shifts from 10  $\mu\text{m}$  (for a nozzle-to-surface distance of 0.15 m) to 20  $\mu\text{m}$  (for a nozzle-to-surface distance of 0.3 m) to 75  $\mu\text{m}$  (for a nozzle-to-surface distance of 0.6 m). As the water flow rate decreases for the same amount of air flow rate, as shown in Figs. 9(b), 9(d), and 9(f), the optimal droplet size required to achieve maximum cooling increases. Less water flow rate results in lower droplets number density and lower incoming momentum. As a result, larger droplets are required to maintain the cooling enhancement factor at maximum level.

Figs. 9(a) through 9(f) show maximum surface wetting is achieved when using sprays that disperse droplets larger than those required to optimize the heat transfer enhancement. For certain air-mist chilling applications such as beef carcasses, optimizing both the droplets surface wetting and the heat transfer is essential. Surface wetting by water droplets helps to minimize the amount of carcass mass loss due to the effect of dehydration. When the beef carcass is sectioned, a red solution of proteins referred to as drip oozes out from the cut surface. Research indicates that a beef carcass can lose up to 1.5% of weight during chilling due to the dripping effect [9-13]. The water-film that covers the carcass surface during air-mist spraying will allow some water to penetrate through the carcass surface pores to regain some of the weight loss.

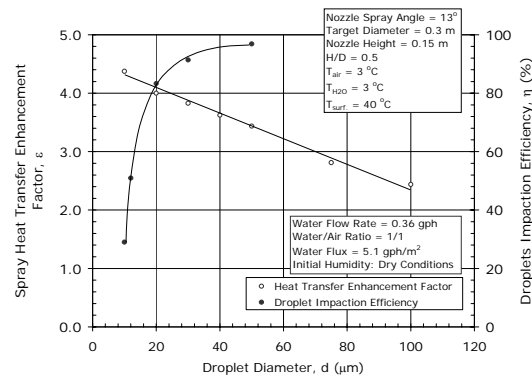


Fig. 9 (a) Heat transfer enhancement factor and droplet impaction efficiency versus droplet diameter ( $H = 0.15 \text{ m}$ ,  $D = 0.3 \text{ m}$ ,  $\phi = 0$ ,  $\psi = 1$ )

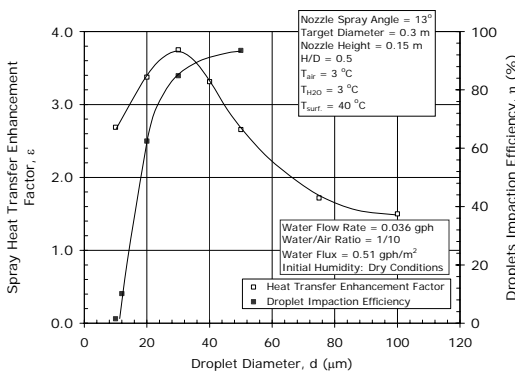


Fig. 9 (b) Heat transfer enhancement factor and droplet impact efficiency versus droplet diameter ( $H = 0.15$  m,  $D = 0.3$  m,  $\phi = 0$ ,  $\psi = 10$ )

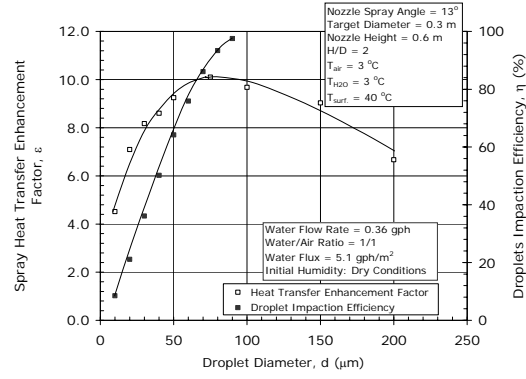


Fig. 9 (e) Heat transfer enhancement factor and droplet impact efficiency versus droplet diameter ( $H = 0.6$  m,  $D = 0.3$  m,  $\phi = 0$ ,  $\psi = 1$ )

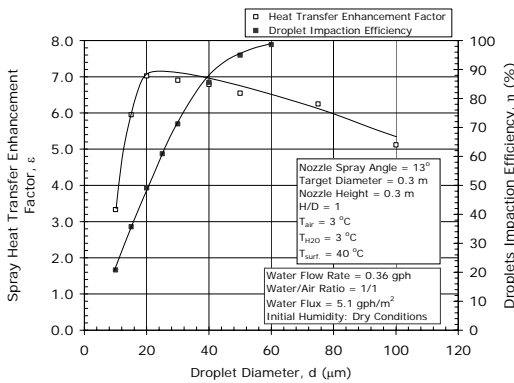


Fig. 9 (c) Heat transfer enhancement factor and droplet impact efficiency versus droplet diameter ( $H = 0.3$  m,  $D = 0.3$  m,  $\phi = 0$ ,  $\psi = 1$ )

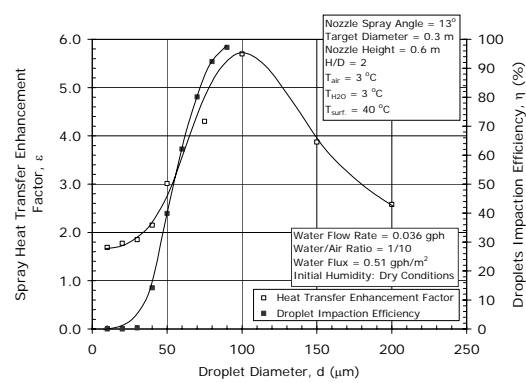


Fig. 9 (f) Heat transfer enhancement factor and droplet impact efficiency versus droplet diameter ( $H = 0.6$  m,  $D = 0.3$  m,  $\phi = 0$ ,  $\psi = 10$ )

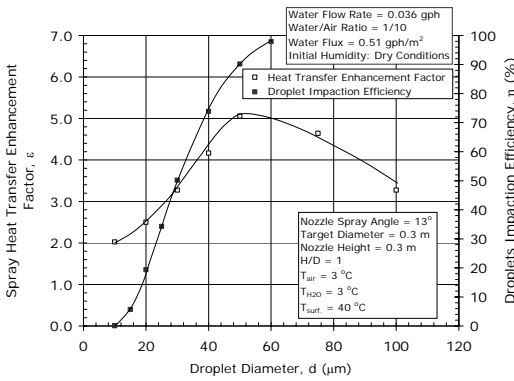


Fig. 9 (d) Heat transfer enhancement factor and droplet impact efficiency versus droplet diameter ( $H = 0.3$  m,  $D = 0.3$  m,  $\phi = 0$ ,  $\psi = 10$ )

To optimize both the heat transfer and surface wetting criteria, a multi-objective optimization methodology can be applied where the net optimal droplet size is between the droplet size required for maximum heat transfer and that required for maximum surface wetting. Let  $P$  be a multiple-objective parameter that needs to be optimized based on weighing factors associated with the heat transfer enhancement ( $f_1$ ) and the droplets impact efficiency ( $f_2$ ) as follows:

$$P = f_1 \frac{\epsilon}{\epsilon_{\max}} + f_2 \frac{\eta}{\eta_{\max}} \quad (9)$$

Where  $\epsilon_{\max}$  and  $\eta_{\max}$  are the maximum heat transfer enhancement factor and droplets impact efficiency, respectively that can be achieved at known operating conditions.

Fig. 10 shows the results from Figs. 9(a) through 9(f) where the multiple-objective parameter,  $P$ , is plotted as function of the spray droplet diameter. Equal weighing factors ( $f_1 = f_2 = 0.5$ ) are used in this case. The results show that  $P$  reaches a maximum at a droplet size larger than that required for maximum heat transfer. The optimal droplet size that is

needed to maximize  $P$  ranges from 30  $\mu\text{m}$  (for  $H=0.15$  m) to 60  $\mu\text{m}$  (for  $H=0.3$  m) to 90  $\mu\text{m}$  (for  $H=0.6$  m).

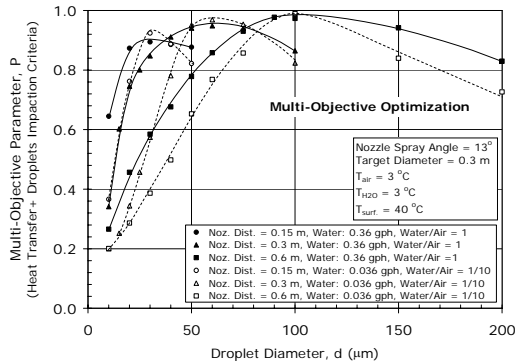


Fig. 10 Multi-objective of heat transfer enhancement and droplets impaction efficiency

### C. Water-Film Accumulation on a Vertical Surface

High water mass flow flux has a detrimental effect on the surface cooling because of the flooding that can occur on the surface. Furthermore, if the spray droplets are too large, there is a risk of water running fast down the chilled surface. In the air-mist chilling of beef carcasses, water runoff on the surface has a detrimental effect on the quality of the processed beef because of the bleached streaks that can be produced on the surface. Therefore, predicting the amount of water flooding on the surface is very critical in the cooling operation.

In the air-mist chilling of beef carcasses, water sprays are intermittently turned ON and OFF. As time elapses while the spraying system is ON, more water droplets accumulate on the surface, where on a vertical surface (as in the case of beef carcass), gravity acts on pulling the water-film downward. When the height of the water-film reaches a critical thickness, gravity overcomes the effect of surface tension and water starts running down the surface. The question of how fast the water-film runs down the surface depends on the size of droplets used in the spray. The droplet size plays a role in the time it takes the water-film to reach maximum speed during runoff. This information provides a clue to what the intermittent spraying time, and the frequency of spraying should be in the chilling operation.

Figs. 11(a) and 11(b) show the water-film mass accumulation and runoff velocity on a vertical surface for sprays having median size droplets of 20 and 100  $\mu\text{m}$ , respectively. A steady high dripping velocity is reached after sufficient water mass has accumulated. This velocity ranges from a creeping velocity of about 2  $\mu\text{m/s}$  for the 20  $\mu\text{m}$  spray droplets size to 7 mm/s for the 100  $\mu\text{m}$  spray. The amount of time required to reach a steady dripping velocity decreases from about 30 s for the 20  $\mu\text{m}$  droplets to about 7 s for the 100  $\mu\text{m}$  droplets. In order to avoid excessive water overflow, the spraying time when large droplets are used should be substantially lower than that for finer droplets.

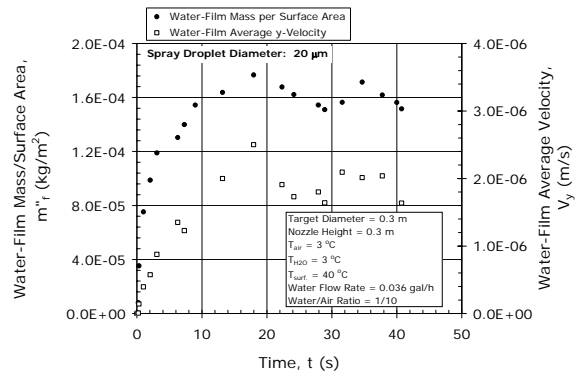


Fig. 11 (a) Water-film surface accumulation versus time ( $d = 20 \mu\text{m}$ )

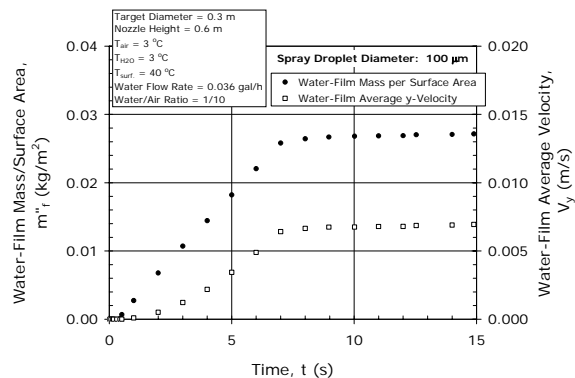


Fig. 11 (b) Water-film surface accumulation versus time ( $d = 100 \mu\text{m}$ )

## VI. CONCLUSION

The transportation process and heat transfer for the air-mist cooling of food products has been simulated using a 2-D numerical model developed using Fluent, a commercially available computational fluid dynamics software. The model takes into consideration droplet-to-surface interaction, droplet evaporation, and water-film accumulation on the surface. Simulations were conducted to evaluate the effect of several parameters on the spray impaction efficiency and the air-mist heat transfer enhancement such as: spray droplet size, air-to-liquid loading, nozzle-to-surface distance, and relative humidity.

Simulation results show that for less dense spray, a noticeable amount of vapor is generated. This amount increases with the decrease in the droplets size. The spray impaction and heat transfer are shown to be dependent on the spray droplet size and flow operating conditions. The optimal droplet size required for maximum impaction is different from that required for maximum heat transfer enhancement.

When saturation conditions prevail, and for  $H/D$  ratios less than or equal to 0.5, the effect of Stokes number on the impaction efficiency is less dependent on the operating conditions for air and water. This is not true when the relative humidity decreases, or  $H/D$  ratio is greater than 0.5. Surface

flooding, especially on a vertical surface, is shown to be controlled by the droplet size in the spray. As the droplet size increases, the velocity of the dripping water-film increases substantially. The rate at which the water-film moves provides an insight into the intermittent spray time and spray frequency needed in actual operation.

The results of the simulations shed light onto the optimal droplet size required to achieve maximum cooling and maximum spray impaction. The selection of this optimal droplet size depends on the spray operating conditions and the location of the nozzle with respect to the surface.

#### REFERENCES

- [1] G. Alvarez, and D. Flick, "Analysis of Heterogeneous Cooling of Agricultural Products Inside Bins – Part I: Aerodynamic Study," *Journal of Food Engineering*, vol. 39, no. 3, pp. 227-237, 1999.
- [2] G. Alvarez, and D. Flick, "Analysis of Heterogeneous Cooling of Agricultural Products Inside Bins – Part II: Thermal Study," *Journal of Food Engineering*, vol. 39, no. 3, pp. 239-245, 1999.
- [3] F. A. Ansari, and S. Y. Khan, "Application Concept of Variable Effective Surface Film Conductance for Simultaneous Heat and Mass Transfer Analysis during Air Blast Cooling of Food," *Energy Conversion and Management*, vol. 40, no. 5, pp. 567-574, 1999.
- [4] S. Chuntranuluck, C. M. Wells, and A. C. Cleland, "Prediction of Chilling Times of Foods in Situations Where Evaporative Cooling is Significant – Part 2. Experimental Testing," *Journal of Food Engineering*, vol. 37, no. 2, pp. 127-141, 1998.
- [5] C. Dirita, M. V. De Bonis, and G. Ruocco, "Analysis of Food Cooling by Jet Impingement Including Inherent Conduction," *Journal of Food Engineering*, vol. 81, no. 1, pp. 12-20, 2007.
- [6] I. Allais, G. Alvarez, and D. Flick, "Modeling Cooling Kinetics of a Stack of Spheres During Mist Chilling," *Journal of Food Engineering*, vol. 72, no. 2, pp. 197-209, 2006.
- [7] I. Allais, and G. Alvarez, "Analysis of Heat Transfer During Mist Chilling of a Packed Bed of Spheres Simulating Foodstuffs," *Journal of Food Engineering*, vol. 49, no. 1, pp. 37-47, 2001.
- [8] P. M. Abdul Majeed, P.M., "Analysis of Heat Transfer during Hydrair Cooling of Spherical Food Products," *International Journal of Heat and Mass Transfer*, vol. 24, pp. 323-333, 1981.
- [9] P. Mallikarjunan, and G. S. Mittal, "Heat and Mass Transfer during Beef Carcass Chilling – Modeling and Simulation," *Journal of Food Engineering*, vol. 23, no. 2, pp. 277-292, 1994.
- [10] A. Kuitche, and J. D. Daudin, "Modeling of Temperature and Weight Loss Kinetics during Meat Chilling for Time-Variable Conditions using an Analytical-Based Method – I. The Model and its Sensitivity to Certain Parameters," *Journal of Food Engineering*, vol. 28, no. 1, pp. 55-84, 1996.
- [11] S. D. M. Jones, and W. M. Robertson, "The Effects of Spray-Chilling Carcasses on the Shrinkage and Quality of Beef," *Meat Science*, vol. 24, no. 3, pp. 177-188, 1988.
- [12] K. J. Kinsella, J. J. Sheridan, T. A. Rowe, F. Butler, A. Delgado, A. Q. Ramirez, I. S. Blair, and D. A. McDowell, "Impact of a Noval Spray-Chilling System on Surface Microflora, Water Activity and Weight Loss during Beef Carcass Chilling," *Food Microbiology*, vol. 23, no. 5, pp. 483-490, 2006.
- [13] P. E. Strydom, and E. M. Buys, "The Effects of Spray-Chilling on Carcass Mass Loss and Surface Associated Bacteriology," *Meat Science*, vol. 39, no. 2, pp. 265-276, 1995.
- [14] M. Fabbri, S. Jiang, and V. K. Dhir, "Comparative Study of Spray and Multiple Micro Jets Cooling for High Power Density Electronic Applications," *Proceedings of IMECE'03, 2003 ASME International Mechanical Engineering Congress and Exposition*, Washington, D.C.
- [15] J. J. Spillman, "Spray Impaction, Retention and Adhesion: an Introduction to Basic Characteristics," *Pesticide Science*, vol. 15, no. 2, pp. 97-106, 1984.
- [16] M. Schatzmann, "Wind Tunnel Modeling of Fog Droplet Deposition on Cylindrical Obstacles," *Journal of Wind Engineering and Industrial Aerodynamics*, vol. 83, no. 1, pp. 371-380, 1999.
- [17] R. J. Issa, and S. C. Yao, "A Numerical Model for Spray-Wall Impactions and Heat Transfer at Atmospheric Conditions," *Journal of Thermophysics and Heat Transfer*, vol. 19, no. 4, pp. 441-447, 2005.
- [18] R. J. Issa, and S. C. Yao, "Modeling of the Mist Dynamics and Heat Transfer at Various Ambient Pressures," *2004 ASME Heat Transfer/Fluids Engineering Summer Conference*.
- [19] D. W. Stanton, and C. J. Rutland, "Multi-Dimensional Modeling of Thin Liquid Films and Spray-Wall Interactions Resulting from Impinging Sprays," *Int. J. Heat Mass Transfer*, vol. 41, no. 20, pp. 3037-3054, 1998.